Los Alamos NATIONAL LABORATORY EST.1943

LA-UR-18-23644 (Accepted Manuscript)

Calibrating Bond-Based Peridynamic Parameters Using a Novel Least Squares Approach

Prakash, Naveen

Provided by the author(s) and the Los Alamos National Laboratory (2018-12-19).

To be published in: Journal of Peridynamics and Nonlocal Modeling

DOI to publisher's version: 10.1007/s42102-018-0002-z

Permalink to record: http://permalink.lanl.gov/object/view?what=info:lanl-repo/lareport/LA-UR-18-23644

Disclaimer:
Approved for public release. Los Alamos National Laboratory, an affirmative action/equal opportunity employer, is operated by the Los Alamos National Security, LLC for the National Nuclear Security Administration of the U.S. Department of Energy under contract DE-AC52-06NA25396. Los Alamos National Laboratory strongly supports academic freedom and a researcher's right to publish; as an institution, however, the Laboratory does not endorse the viewpoint of a publication or guarantee its technical correctness.

RESEARCH LIBRARY

Calibrating bond-based peridynamic parameters using a novel least squares approach

Naveen Prakash[a,]

[a]*Theoretical Division, T-3, Los Alamos National Laboratory*
Los Alamos, New Mexico 87545, USA

Abstract

This work presents a novel procedure to calibrate the bond micromoduli in a discrete bond based peridynamics setting. Conventionally, an analytical expression has been used based on strain energy equivalence. In the present work, the micromoduli for individual bonds in a neighborhood are calibrated by equating the effective peridynamic stiffness to the reference material stiffness and posed as a set of linear system of equations. The solution to this is found by a least squares approach which aims to reduce the error in the components of the stiffness matrix. Results for an isotropic case in a local neighborhood of particles are shown to demonstrate the feasibility of this approach.

Keywords: Peridynamics, Surface Effects, Micromoduli

1. Background and Motivation

Peridynamics is a non-local theory of continuum mechanics which formulates the balance laws in terms of integro differential equations [1]. The advantage of using an integral expression to describe internal forces is that it is valid even in the presence of discontinuities hence making it simpler to model fracture, allowing for spontaneous crack formation propagation. Equations of peridynamics which were originally developed for structural mechanics have been since extended to heat conduction [2, 3], electrical conduction [4, 5], fluid flow [6] and corrosion [7]. The range of problems peridynamics has been applied to extends from dynamic crack branching [8, 9] to damage in composite materials [10], concrete structures[11] and nanocomposites[12], hydraulic fracturing [13] and many others.

In the theory of peridynamics, every material particle $\boldsymbol{x}$ in the continuum is assumed to interact with every other particle $\boldsymbol{x'}$ within some region of influence called the horizon $\mathcal{H}_{\boldsymbol{x}}$ through a *peridynamic bond*. Consider two particles $\boldsymbol{x}$ and $\boldsymbol{x'}$ in the reference configuration separated by their relative distance $\boldsymbol{\xi} = \boldsymbol{x'} - \boldsymbol{x}$. If $\boldsymbol{x}$ and $\boldsymbol{x'}$ are displaced by $\boldsymbol{u}$ and $\boldsymbol{u'}$ respectively, their relative displacement is given by $\boldsymbol{\eta} = \boldsymbol{u'} - \boldsymbol{u}$ such that their relative position in the deformed configuration is given by $\boldsymbol{\xi} + \boldsymbol{\eta}$.

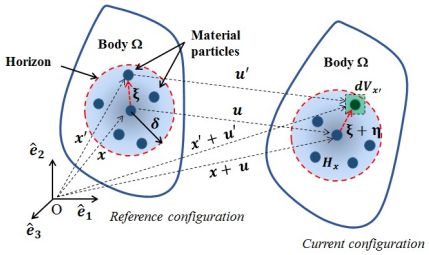

Figure 1: Kinematics of peridynamic material particles, material particle $\boldsymbol{x}$ and $\boldsymbol{x'}$ correspond to an interacting pair of particles within the horizon region of $\boldsymbol{x}$, having a volume $dV_{\boldsymbol{x'}}$ [14].

Email address: n.prakash@lanl.gov (Naveen Prakash)

The peridynamic equation of motion for a particle $\boldsymbol{x}$ at time t is given by,

$$\rho\ddot{\boldsymbol{u}}(\boldsymbol{x},t) = \int_{\mathcal{H}_x} \boldsymbol{f}(\boldsymbol{u}',\boldsymbol{u},\boldsymbol{x}',\boldsymbol{x},t)dV_{x'} + \boldsymbol{b}(\boldsymbol{x},t), \tag{1}$$

where ρ and $\ddot{\boldsymbol{u}}$ denote the density and acceleration of the material particle $\boldsymbol{x}$, $\boldsymbol{f}$ is known as the pairwise force function (units of force per unit volume squared) of the bond between $\boldsymbol{x}$ and $\boldsymbol{x}'$ and $\boldsymbol{b}$ is the body force per unit volume at $\boldsymbol{x}$, all at time t. The net internal force per unit volume arising from pairwise interactions of particles is obtained from the integral of $\boldsymbol{f}$ over the horizon $\mathcal{H}_x$ where $dV_{x'}$ has the meaning of the differential volume element about the particle $\boldsymbol{x}'$ which is the subset of the volume of the horizon region of $\boldsymbol{x}$. Since the formulation does not involve spatial derivatives of displacement, the same governing equations can be applied in the presence of discontinuities. Assuming that the pairwise force function depends only on the reference separation of the particles $\boldsymbol{x}' - \boldsymbol{x}$ and the relative displacement $\boldsymbol{u}' - \boldsymbol{u}$, equation (1) then reduces to,

$$\rho\ddot{\boldsymbol{u}}(\boldsymbol{x},t) = \int_{\mathcal{H}_x} \boldsymbol{f}(\boldsymbol{u}' - \boldsymbol{u},\boldsymbol{x}' - \boldsymbol{x},t)dV_{x'} + \boldsymbol{b}(\boldsymbol{x},t), \tag{2}$$

or in other words,

$$\rho\ddot{\boldsymbol{u}}(\boldsymbol{x},t) = \int_{\mathcal{H}_x} \boldsymbol{f}(\boldsymbol{\eta},\boldsymbol{\xi},t)dV_{x'} + \boldsymbol{b}(\boldsymbol{x},t). \tag{3}$$

According to Silling [1], a micro-elastic material is defined as one in which the internal force is the gradient of a scalar potential $w(\boldsymbol{\eta},\boldsymbol{\xi})$ i.e.,

$$\boldsymbol{f}(\boldsymbol{\eta},\boldsymbol{\xi},t) = \frac{\partial w(\boldsymbol{\eta},\boldsymbol{\xi})}{\partial \boldsymbol{\eta}}. \tag{4}$$

For an elastic material, the scalar potential refers to a micro-elastic strain energy, i.e. strain energy density per unit volume stored in the material. The material is said to be linear micro-elastic[1] if w is chosen to be,

$$w(\boldsymbol{\xi},\boldsymbol{\eta}) = \frac{c(\boldsymbol{\xi})s^2(\boldsymbol{\eta},\boldsymbol{\xi})|\boldsymbol{\xi}|}{2}, \tag{5}$$

where $c(\boldsymbol{\xi})$ is a constant called the micromodulus, $|\boldsymbol{\xi}|$ is the magnitude of the reference bond vector $\boldsymbol{\xi}$ and s is the stretch of the bond which is given by,

$$s = \frac{|\boldsymbol{\xi}+\boldsymbol{\eta}| - |\boldsymbol{\xi}|}{|\boldsymbol{\xi}|}. \tag{6}$$

The micromodulus $c(\boldsymbol{\xi})$ can depend on the reference bond vector $\boldsymbol{\xi}$, however for homogeneous isotropic materials the micromodulus is assumed to be independant of the direction of the bond. If Eq. (5) is substituted in Eq. (4), the expression for the internal force density in a peridynamic bond for a homogeneous linear isotropic material can be derived such that the internal force $\boldsymbol{f}$ is given by,

$$\boldsymbol{f}(\boldsymbol{\eta},\boldsymbol{\xi}) = cs\frac{\boldsymbol{\xi}+\boldsymbol{\eta}}{|\boldsymbol{\xi}+\boldsymbol{\eta}|}, \tag{7}$$

where the force in the bond is a function of the stretch of the bond s, the micromodulus c and acts in the direction of the deformed bond as indicated by the unit vector $(\boldsymbol{\xi}+\boldsymbol{\eta})\,/\,(|\boldsymbol{\xi}+\boldsymbol{\eta}|)$. This is commonly known as the *linear microelastic* model of peridynamics and the reader is referred to Silling[1, 15] for a detailed derivation of $\boldsymbol{f}$ and Eq. (7). In this general form, bond stretch is a nonlinear function of $\boldsymbol{u}' - \boldsymbol{u}$, the relative displacement of the bond and hence the force - displacement relationship is nonlinear. This constitutive model can be linearized by assuming small deformations, i.e. $\eta \ll 1$ and the force can be written as [14],

$$\boldsymbol{f}(\boldsymbol{\eta},\boldsymbol{\xi}) = c\frac{\eta_n}{|\boldsymbol{\xi}|}\frac{\boldsymbol{\xi}}{|\boldsymbol{\xi}|}, \tag{8}$$

where η_n denotes the component of relative displacement in the direction of the undeformed bond. Comparing Eq. (8) to Eq. (7), it is found that the term $\eta_n/|\boldsymbol{\xi}|$ is the linearized stretch s and the direction of the force is changed

from the deformed bond direction to the undeformed bond direction. Substituting for the internal force density from Eq. (8) in Eq. (3), the peridynamic linear momentum equation with a linearized force - displacement relationship becomes,

$$\rho\ddot{\boldsymbol{u}}(\boldsymbol{x},t) = \int_{\mathcal{H}_x} c\frac{\eta_n}{|\boldsymbol{\xi}|}\frac{\boldsymbol{\xi}}{|\boldsymbol{\xi}|}dV_{\boldsymbol{x}'} + \boldsymbol{b}(\boldsymbol{x},t). \tag{9}$$

1.1. Calibrating the Micromodulus

The micromodulus can be evaluated by comparing the stored peridynamic strain energy density to that obtained using classical continuum mechanics principles. The '*macroelastic*' peridynamic strain energy density W^{PD} stored at $\boldsymbol{x}$ is obtained by integrating w over the horizon $\mathcal{H}_x$ of $\boldsymbol{x}$, i.e. integrating over all bonds connected to $\boldsymbol{x}$,

$$W^{PD}(\boldsymbol{x}) = \frac{1}{2}\int_{\mathcal{H}_x} w dV_{\boldsymbol{x}'}, \tag{10}$$

where the $1/2$ appears because it is assumed that each particle stores half of the microelastic strain energy in the bond connecting two particles. Using the linearized stretch, the microelastic strain energy density can then be written as,

$$w = \frac{1}{2}\frac{c\eta_n^2}{|\boldsymbol{\xi}|}. \tag{11}$$

Integrating over the horizon $\mathcal{H}_x$ of the particle $\boldsymbol{x}$ to obtained the macroelastic strain energy density,

$$W^{PD}(\boldsymbol{x}) = \frac{1}{2}\int_{\mathcal{H}_x}\frac{1}{2}\frac{c\eta_n^2}{|\boldsymbol{\xi}|}dV_{\boldsymbol{x}'}. \tag{12}$$

For example in 2D, assuming that the horizon region for every particle $\boldsymbol{x}$ is a circular region of a fixed radius δ around the particle, converting to polar coordinates and changing the limits,

$$W^{PD}(\boldsymbol{x}) = \frac{c}{4}\int_0^{2\pi}\int_0^{\delta}\frac{\eta_n^2}{\xi}\xi d\xi d\theta, \tag{13}$$

where the convention $\xi = |\boldsymbol{\xi}|$ is used for simplicity. Eq. (13) simplifies to,

$$W^{PD}(\boldsymbol{x}) = \frac{c}{4}\int_0^{2\pi}\int_0^{\delta}\eta_n^2 d\xi d\theta. \tag{14}$$

The peridynamic strain energy density for a material particle can now be evaluated for a homogeneous deformation such that the relative displacement η_n can be written in terms of the imposed strains.

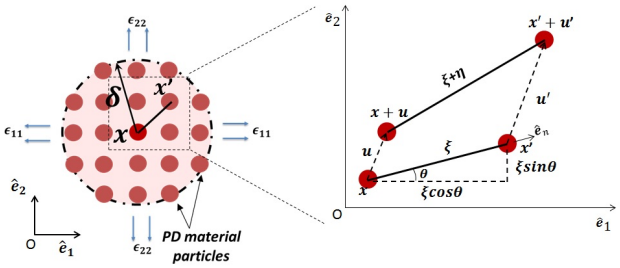

Figure 2: Schematic of a peridynamic body under a prescribed strain field (left) and the deformation of the bond connecting $\boldsymbol{x}$ and $\boldsymbol{x}'$ under the prescribed field [14]

.

Consider an isotropic homogeneous body under a homogeneous bi-axial strain field as shown in Figure 2. Assuming infinitesimal strains, the relative displacement η_n can be written in terms of the imposed strains ε_{11} and ε_{22} as [14],

$$\eta_n = \xi(\varepsilon_{11}\cos^2\theta + \varepsilon_{22}\sin^2\theta). \tag{15}$$

Substituting this in Eq. (14),

$$W^{PD}(\boldsymbol{x}) = \frac{c}{4}\int_0^{2\pi}\int_0^{\delta}(\varepsilon_{11}\cos^2\theta + \varepsilon_{22}\sin^2\theta)^2\xi^2 d\xi d\theta. \tag{16}$$

Assuming further that $\varepsilon_{11} = \varepsilon_{22} = \varepsilon$ and integrating with respect to ξ and θ, Eq. (16) becomes,

$$W^{PD}(\boldsymbol{x}) = \frac{\pi c\delta^3\varepsilon^2}{6}. \tag{17}$$

Under 2D plane stress conditions, the strain energy density according to classical elasticity is,

$$W^{CCM}(\boldsymbol{x}) = \frac{E}{2(1-\nu^2)}\left(\varepsilon_{11}^2 + \varepsilon_{22}^2\right) + \frac{E\nu}{1-\nu^2}\varepsilon_{11}\varepsilon_{22}. \tag{18}$$

For strains $\varepsilon_{11} = \varepsilon_{22} = \varepsilon$, Eq. (18) becomes,

$$W^{CCM}(\boldsymbol{x}) = \frac{E\varepsilon^2}{(1-\nu)}. \tag{19}$$

The peridynamic strain energy density given in Eq. (17) must equal that obtained from classical elasticity given in Eq. (19). Equating these two, the expression for the micromodulus c can be derived as,

$$c = \frac{6E}{\pi\delta^3(1-\nu)}, \tag{20}$$

where E and ν are the classical continuum mechanics definitions of Young's modulus and Poisson's ratio for a linear elastic material. Similarly, the micromodulus under plane strain conditions can be derived as,

$$c = \frac{6E}{\pi\delta^3(1+\nu)(1-2\nu)}, \tag{21}$$

and in 3D can be evaluated to be [16],

$$c^{3D} = \frac{18K}{\pi\delta^4}. \tag{22}$$

2. Issues with Peridynamics Parameters and Numerical Implementation

It is now well known that the biggest shortcoming of bond based peridynamics, much like many other spring lattice models is the issue of inaccurate elastic properties. Since these models are based on central forces, i.e. forces can only be in the direction of the bond, and shear forces are not allowed unlike in classical continuum mechanics, this limits the range of elastic properties that can be modeled [1, 17–20].

Silling and Askari [16] derived the micromodulus constant in 3D by assuming an isotropic expansion case where all bonds are assumed to elongate by an equal amount in the reference direction of the bond, i.e. $\boldsymbol{\eta} = s\boldsymbol{\xi}$. The resulting expression for micromodulus constant is in terms of the bulk modulus of the material K,

$$c_{3D} = \frac{18K}{\pi\delta^4}. \tag{23}$$

A similar expression can be derived in 2D by using the relation,

$$K_{2D} = \frac{E}{2(1-\nu)}. \tag{24}$$

Substituting Eq. (24) in Eq. (20) one obtains the expression,

$$c_{2D} = \frac{12K_{2D}}{\pi\delta^3}. \tag{25}$$

which was first derived in Gerstle et al. [11] and later in Ha et al. [8, 21]. It is observed from Eqs. (23) and (25) that there is a one to one correspondence of micromodulus constant with the bulk modulus of the material, but not with other material constants like the Young's modulus and Poisson's ratio ν. This relation between the micromodulus and the elastic constants and the calibration of the micromodulus affects the representation of strain energy in the peridynamic model. In other words, for any general biaxial test where ε_{11} is not necessarily equal to ε_{22}, the peridynamic strain energy is not equal to the classical continuum mechanics strain energy unless $\nu = 1/3$. Similarly, the Poisson's ratio is restricted to 1/4 in 2D plane strain and 3D. This effect is not only restricted to the Poisson's ratio but also manifests in the effective Young's modulus.

Apart from the errors due to the calibration of peridynamic parameters, there are also errors accrued due to what are known as 'surface effects'. Relationships between peridynamic parameters and classical continuum properties are derived using strain energy equivalence by assuming that the requisite particle is in the bulk, i.e. the integral in Eq. (10) is over a full circular region. However, if the parameters derived using this assumption are used for particles near a boundary for which it's horizon is incomplete, e.g. a particle at the corner of a rectangular domain (2D) that has only a fourth of it's horizon occupied by material particles, the effective material properties for such a particle are different from those obtained in the bulk. This can have a huge effect on the accuracy of the solution, for example Le at al. have shown in 2D uniaxial simulations that the difference in displacements when compared to the classical solution can be up to ~26% and ~96% at corners in the axial and transverse directions respectively. This is true not only for elastic properties but also for fracture properties, not only for particles near an outer edge but also for particles near features such as a hole or a cut-out and at a crack surface or a crack tip or at a material interface. It is also expected that these errors are compounded when the material being modeled is anisotropic such as a tranversely isotropic unidirectional fiber composite.

Some methods have been proposed over the years to counteract this effect. Macek and Silling provided a method to correct for surface forces called the force normalization procedure by scaling the analytical micromodulus with a constant depending on restoring force near the surface in contrast with the restoring force near the bulk [22]. A somewhat similar method was proposed by Oterkus and Madenci [23, 24] based on the strain energy stored in the bulk of the material versus that near an edge. A more straightforward scaling of the micromodulus based on the ratio of horizon volumes near an edge and in the bulk is given in [25]. The position aware linear solid model (PALS) proposed by Mitchell at al. [26] for linear peridynamic state-based model relies on modifying the influence function for counteracting the surface effect, which has been provided with a slight modification in [27]. Of course, the need for modifications of the force function can be circumvented by adding a few layers of fictitious/ghost nodes around the boundary instead [11]. The summary of all these methods and more can be found in this excellent review by Le et al. [27].

There are also some errors introduced due to partial volumes also referred to here as 'volume effects' introduced due to the meshfree quadrature scheme generally used to discretize the PD equations. The analytical micromodulus is evaluated by integrating over a circle in 2D and sphere in 3D (most commonly). However, even in the bulk the summation of discrete nodal volumes is generally not equal to original volume of integration when the micromodulus was derived, i.e. $\sum \Delta V_{\boldsymbol{x}'} \neq \int_{\mathcal{H}_{\boldsymbol{x}}} dV_{\boldsymbol{x}'}$. Correction schemes for this have been introduced in [28], [29] based on correction of nodal volumes at the boundary of the neighborhood. Yu et al. presented a highly detailed scheme depending on the type of intersection of the horizon with the particles near the edge of the neighborhood. Similarly, Seleson presented a detailed study comparing a number of existing techniques and presented an improved method to counter volume effects in [30]. Another option is to employ a radially decaying force function such that the effect of nodal volumes near the edge of the neighborhood is reduced [31]. Liu and Hong [32, 33] instead chose to calibrate the micromodulus in a discrete sense and provide analytical expressions in 3D for various values of the horizon. Ganzemuller et al. [34] also propose a similar discrete calibration of the micromodulus and showed improvements over the analytical version in both static and dynamic cases.

3. Optimizing peridynamic parameters

The authors propose a 'reverse engineered' calibration of peridynamic parameters in this manuscript which is aimed at numerical calibration of peridynamic bond properties at each point in the domain through an optimization approach, which is expected to account for volume and surface corrections, and be agnostic to anisotropy of the material being modeled (within limitations of the bond based theory).

Assuming small strains and displacement and linear elastic response, the macroelastic strain energy density under a homogeneous strain field is given by Eq. 12,

$$W^{PD}(\boldsymbol{x}) = \frac{1}{2}\int_{\mathcal{H}_x}\frac{1}{2}\frac{c\eta_n^2}{|\boldsymbol{\xi}|}dV_{\boldsymbol{x}'}. \tag{26}$$

Taking the derivative with respect to strain,

$$\frac{\partial W^{PD}}{\partial \varepsilon_{kl}} = \frac{1}{2}\int_{\mathcal{H}_x}\frac{c\eta_n}{|\boldsymbol{\xi}|}\frac{\partial \eta_n}{\partial \varepsilon_{kl}}dV_{\boldsymbol{x}'}, \tag{27}$$

where the relative displacement can be written in terms of the bond length and the strain field as,

$$\eta_n = \left(\frac{\xi_i \varepsilon_{ij}\xi_j}{|\boldsymbol{\xi}|}\right), \tag{28}$$

and the derivative can be written as,

$$\frac{\partial \eta_n}{\partial \varepsilon_{kl}} = \frac{\xi_k \varepsilon_{kl}\xi_l}{|\boldsymbol{\xi}|}. \tag{29}$$

Substituting in Eq. 27 and taking the derivative again,

$$\frac{\partial W^{PD}}{\partial \varepsilon_{ij}\partial \varepsilon_{kl}} = \int_{H_x}\frac{c}{2}\frac{\xi_i\xi_j\xi_k\xi_l}{|\boldsymbol{\xi}|^3}dV_{\boldsymbol{x}'}. \tag{30}$$

which is nothing but the fourth order stiffness tensor,

$$\mathbb{C}^{per}_{ijkl} = \int_{H_x}\frac{c}{2}\frac{\xi_i\xi_j\xi_k\xi_l}{|\boldsymbol{\xi}|^3}dV_{\boldsymbol{x}'}, \tag{31}$$

or in vector notation can be written as,

$$\mathbf{C}^{per} = \int_{H_x}\frac{c}{2}\frac{\boldsymbol{\xi}\otimes\boldsymbol{\xi}\otimes\boldsymbol{\xi}\otimes\boldsymbol{\xi}}{|\boldsymbol{\xi}|^3}dV_{\boldsymbol{x}'}, \tag{32}$$

where the integral is over the horizon of particle $\boldsymbol{x}$ which covers an infinite number of it's neighbors $\boldsymbol{x}'$ and the range of indices ijkl are from 1 to 3. The discrete version for a discretized domain can be written by regarding the integral as a finite summation following the method of Silling and Askari [16] in indicial notation as,

$$\mathbb{C}^{per}_{ijkl} = \sum_{N=1}^{M}\frac{c^N}{2}\frac{\xi_i^N\xi_j^N\xi_k^N\xi_l^N}{|\boldsymbol{\xi}|^3}\Delta V_N, \tag{33}$$

where this expression is written for the particle $\boldsymbol{x}$ as a summation over it's Nth neighbor where N varies from 1 to M, where M is the total number of neighbors, and therefore bonds. For example, the stiffness term $\mathbb{C}^{p}_{1111}$ can be written as,

$$\mathbb{C}^{per}_{1111} = \sum_{N=1}^{M}\frac{c^N}{2}\frac{\xi_1^N\xi_1^N\xi_1^N\xi_1^N}{|\boldsymbol{\xi}|^3}\Delta V_N. \tag{34}$$

To simplify, we can choose to work in Voigt notation, where by taking advantage of minor and major symmetries, the fourth order stiffness tensor can be written as a 6×6 matrix. Therefore Eq. (33) can be written in terms of the Voigt indices as,

$$\mathbb{C}^{per}_{\alpha\beta} = \sum_{N=1}^{M}\frac{c^N}{2}\frac{\zeta_\alpha^N\zeta_\beta^N}{|\boldsymbol{\xi}|^3}\Delta V_N. \tag{35}$$

where α and β are the two Voigt indices that vary from 1 to 6 such that they relate to cartesian indices $ijkl$ as: 1→11, 2→22, 3→33, 4→23, 5→31 and 6→12. For example $\mathbb{C}_{56}$ in Voigt notation corresponds to $\mathbb{C}_{3112}$ in conventional

notation, or $\mathbb{C}_{1312}$ due to minor symmetry. Similarly, $\zeta_1 = \xi_1\xi_1$, $\zeta_2 = \xi_2\xi_2$, $\zeta_1 = \xi_3\xi_3$, $\zeta_4 = \xi_2\xi_3$, $\zeta_5 = \xi_1\xi_3$ and $\zeta_6 = \xi_1\xi_2$.

For each one of the 21 independent constants, Eq. (35) can be written as a dot product of two vectors,

$$\mathbb{C}^{per}_{\alpha\beta} = \left[\sum_{N=1}^{M} \frac{1}{2} \frac{\zeta^N_\alpha \zeta^N_\beta}{|\boldsymbol{\xi}|^3} \Delta V_N\right] c^N. \tag{36}$$

where the length of the vectors are equal to the number of neighbors or the number of bond micromoduli to be evaluated - M. For example, for the 11 component,

$$\left[\mathbb{C}^{per}_{11}\right] = \begin{bmatrix} \frac{1}{2}\frac{\zeta^1_1\zeta^1_1}{|\boldsymbol{\xi}|^3}\Delta V_1 & \frac{1}{2}\frac{\zeta^2_1\zeta^2_1}{|\boldsymbol{\xi}|^3}\Delta V_2 & \frac{1}{2}\frac{\zeta^3_1\zeta^3_1}{|\boldsymbol{\xi}|^3}\Delta V_3 & \cdots & \frac{1}{2}\frac{\zeta^N_1\zeta^N_1}{|\boldsymbol{\xi}|^3}\Delta V_M \end{bmatrix} \begin{bmatrix} c^1 \\ c^2 \\ c^3 \\ \vdots \\ c^M \end{bmatrix}. \tag{37}$$

If the 21 independent stiffness components $\mathbb{C}^{per}_{\alpha\beta}$ are arranged as components of a vector $[\mathbb{C}^{per}_{11}\ \mathbb{C}^{per}_{12}\ \mathbb{C}^{per}_{13}\ ...\ \mathbb{C}^{per}_{66}]^T$ then,

$$\begin{bmatrix} \mathbb{C}^{per}_{11} \\ \mathbb{C}^{per}_{12} \\ \mathbb{C}^{per}_{13} \\ \vdots \\ \mathbb{C}^{per}_{66} \end{bmatrix} = \begin{bmatrix} \frac{1}{2}\frac{\zeta^1_1\zeta^1_1}{|\boldsymbol{\xi}|^3}\Delta V_1 & \frac{1}{2}\frac{\zeta^2_1\zeta^2_1}{|\boldsymbol{\xi}|^3}\Delta V_2 & \frac{1}{2}\frac{\zeta^3_1\zeta^3_1}{|\boldsymbol{\xi}|^3}\Delta V_3 & \cdots & \frac{1}{2}\frac{\zeta^N_1\zeta^N_1}{|\boldsymbol{\xi}|^3}\Delta V_M \\ \frac{1}{2}\frac{\zeta^1_1\zeta^1_2}{|\boldsymbol{\xi}|^3}\Delta V_1 & \frac{1}{2}\frac{\zeta^2_1\zeta^2_2}{|\boldsymbol{\xi}|^3}\Delta V_2 & \frac{1}{2}\frac{\zeta^3_1\zeta^3_2}{|\boldsymbol{\xi}|^3}\Delta V_3 & \cdots & \frac{1}{2}\frac{\zeta^N_1\zeta^N_2}{|\boldsymbol{\xi}|^3}\Delta V_M \\ \frac{1}{2}\frac{\zeta^1_1\zeta^1_3}{|\boldsymbol{\xi}|^3}\Delta V_1 & \frac{1}{2}\frac{\zeta^2_1\zeta^2_3}{|\boldsymbol{\xi}|^3}\Delta V_2 & \frac{1}{2}\frac{\zeta^3_1\zeta^3_3}{|\boldsymbol{\xi}|^3}\Delta V_3 & \cdots & \frac{1}{2}\frac{\zeta^N_1\zeta^N_3}{|\boldsymbol{\xi}|^3}\Delta V_M \\ \vdots & \vdots & \vdots & \vdots & \vdots \\ \frac{1}{2}\frac{\zeta^1_6\zeta^1_6}{|\boldsymbol{\xi}|^3}\Delta V_1 & \frac{1}{2}\frac{\zeta^2_6\zeta^2_6}{|\boldsymbol{\xi}|^3}\Delta V_2 & \frac{1}{2}\frac{\zeta^3_6\zeta^3_6}{|\boldsymbol{\xi}|^3}\Delta V_3 & \cdots & \frac{1}{2}\frac{\zeta^N_6\zeta^N_6}{|\boldsymbol{\xi}|^3}\Delta V_M \end{bmatrix} \begin{bmatrix} c^1 \\ c^2 \\ c^3 \\ \vdots \\ c^N \end{bmatrix}, \tag{38}$$

or in matrix notation can be written as,

$$\tilde{\mathbf{C}}^{per} = \mathbf{X}\boldsymbol{c}, \tag{39}$$

where tilde is used to denote that the stiffness components are written in vector form. If the desired elastic stiffness of the material or the 'reference' stiffness is similarly denoted by $\tilde{\mathbf{C}}^{ref}$, then ideally, the aim would be to enforce exactly $\tilde{\mathbf{C}}^{ref} = \tilde{\mathbf{C}}^{per}$. However, since the number of bonds micromoduli to be calibrated will in general far exceed the number of independent continuum stiffness terms, this is a underdetermined system and in general a unique solution does not exist. Hence the solution, i.e. $\boldsymbol{c}$ that we aim to find is the one with the least error in a least-squares sense, that is,

$$\boldsymbol{c} = \boldsymbol{c} : c_i \geq 0, min \left\|\tilde{\mathbf{C}}^{ref} - \mathbf{X}\boldsymbol{c}\right\|^2. \tag{40}$$

An additional constraint that is imposed is that for the strain energy stored by a bond is always greater than or equal to zero, the bond micromoduli have to be non-negative.

One way to find a unique solution to the problem is find that solution to the least squares problem which gives the lowest value of micromoduli. In other words, to find the minimum norm least squares solution where in addition to minimizing the residual given by $\left\|\tilde{\mathbf{C}}^{ref} - \mathbf{X}\boldsymbol{c}\right\|^2$, the norm of the solution $\|\boldsymbol{c}\|$ itself is minimized. This can be computed from the Moore-Penrose pseudoinverse of $\mathbf{X}$ (in a software such as MATLAB, the functions *pinv* or *lsqminnorm* can be used to compute this solution). However, this does not guarantee the non-negativity of the solution. Therefore to find the solution with the least norm and least residual within the space of positive solutions, the following scheme is proposed.

Let $\boldsymbol{v}$ be a vector of size M $\times$ 1 such that it lies in the null space of $\mathbf{X}$ such that,

$$\mathbf{X}\boldsymbol{v} = \mathbf{0}. \tag{41}$$

Then the desired is solution is the vector $\boldsymbol{c} + \boldsymbol{v}$ such that the norm $\|\boldsymbol{c} + \boldsymbol{v}\|$ is minimum and non-negative, $\boldsymbol{c} + \boldsymbol{v} \geq \mathbf{0}$. In other words, the desired solution is obtained by first solving for the minimum norm least squares solution $\boldsymbol{c}$. Following this, the solution $\boldsymbol{c}$ is perturbed by an amount $\boldsymbol{v}$ such that $\boldsymbol{c} + \boldsymbol{v}$ is non-negative and the residual $\left\|\tilde{\mathbf{C}}^{ref} - \mathbf{X}(\boldsymbol{c} + \boldsymbol{v})\right\|^2$

remains unchanged since $\boldsymbol{v}$ lies in the null space of $\mathbf{X}$. This scheme can be posed as a quadratic program subject to linear equality and inequality constraints as follows,

Finding $min\,\|\boldsymbol{c}+\boldsymbol{v}\|$ is equivalent to finding the $min\,\frac{1}{2}(\boldsymbol{c}+\boldsymbol{v})^T(\boldsymbol{c}+\boldsymbol{v})$ which can be expanded as,

$$min\,\frac{1}{2}(\boldsymbol{c}+\boldsymbol{v})^T(\boldsymbol{c}+\boldsymbol{v}) = min\,\frac{1}{2}\left(\boldsymbol{c}^T\boldsymbol{c}+\boldsymbol{v}^T\boldsymbol{c}+\boldsymbol{c}^T\boldsymbol{v}+\boldsymbol{v}^T\boldsymbol{v}\right), \tag{42}$$

$$= min\,\frac{1}{2}\boldsymbol{v}^T\boldsymbol{v}+\boldsymbol{c}^T\boldsymbol{v}, \tag{43}$$

$$= min\,\frac{1}{2}\boldsymbol{v}^T\boldsymbol{I}\boldsymbol{v}+\boldsymbol{c}^T\boldsymbol{v}, \tag{44}$$

where $\boldsymbol{I}$ is an M × M identity matrix and the term $\boldsymbol{c}^T\boldsymbol{c}$ is dropped since it is a known positive constant and does not affect the minimum. Therefore, the quadratic program can be now written as,

$$Minimize \quad \frac{1}{2}\boldsymbol{v}^T\boldsymbol{I}\boldsymbol{v}+\boldsymbol{c}^T\boldsymbol{v}; \tag{45}$$

$$Subject\ to \quad \boldsymbol{c}+\boldsymbol{v}\geq\mathbf{0}, \tag{46}$$

$$\mathbf{X}\boldsymbol{v}=\mathbf{0}. \tag{47}$$

This problem is trivial to solve in an application such as MATLAB using the *quadprog* function by providing the necessary matrices.

Note that in the first step, other routines such as *lsqlin* and *lsqnonneg* can also be used to obtain the original solution $\boldsymbol{c}$, which may return one of multiple solutions for $\boldsymbol{c}$. For example, using *lsqnonneg* returns a solution of non-negative values in the solution vector but not necessarily of minimum norm. However, this is rendered moot as the second step aims to find the minimum norm solution $(\boldsymbol{c}+\boldsymbol{v})$ which is cast as the objective function to be minimized in the quadratic program. The minor advantage of using say, *lsqminnorm* in the first step is that if for a particular case, this routine finds the minimum norm solution will all non-negative micromoduli, that is *the* desired solution and the need for the second step is eliminated.

The results in the following section were generated using the *lsqnonneg* routine in MATLAB R2017b using a 64-bit Intel core i5 5300 processor. By default the tolerance for this routine is on the order of $\sim 10\epsilon$ where machine precision ϵ in MATLAB is 2.2204e-16.

4. Results and Discussion

4.1. Poisson's ratio = 0.25

For the purposes of demonstrating this method, a reference peridynamic particle with a spherical neighborhood is considered. For the sake of simplicity, quantities are considered to be unity wherever possible. For example, each particle is assumed to be seeded at the center of a cube of length unity and therefore of volume unity. The same is assumed for neighboring particles, which are spaced at a nearest neighbor distance of unity from each other.

The simplest and the most general case, an isotropic material is considered first. The Young's modulus is considered to be 1.0 and the Poisson's ratio is considered to be 0.25 such that the stiffness matrix in Voigt notation is as follows:

$$\mathbf{C}_{iso}^{ref} = \begin{bmatrix} 1.2 & 0.4 & 0.4 & 0 & 0 & 0 \\ 0.4 & 1.2 & 0.4 & 0 & 0 & 0 \\ 0.4 & 0.4 & 1.2 & 0 & 0 & 0 \\ 0 & 0 & 0 & 0.4 & 0 & 0 \\ 0 & 0 & 0 & 0 & 0.4 & 0 \\ 0 & 0 & 0 & 0 & 0 & 0.4 \end{bmatrix}. \tag{48}$$

The bond micromoduli are solved for using the least squares (LS) approach proposed in section 3 for horizon δ equal to 1, 2, 2.5 and 3. For the purposes of illustration, the particles are depicted as colored spheres in Figure 3 with the color depicting the magnitude of bond micromodulus between a particular particle in the lattice and the reference particle at the center of the lattice. Unlike evaluating a single value for the micromodulus using the analytical expression given

in Eq. (23), the least squares approach gives multiple values of bond micromoduli, even in the isotropic case. The bond micromoduli obtained for various values of horizon is given in Figure 3.

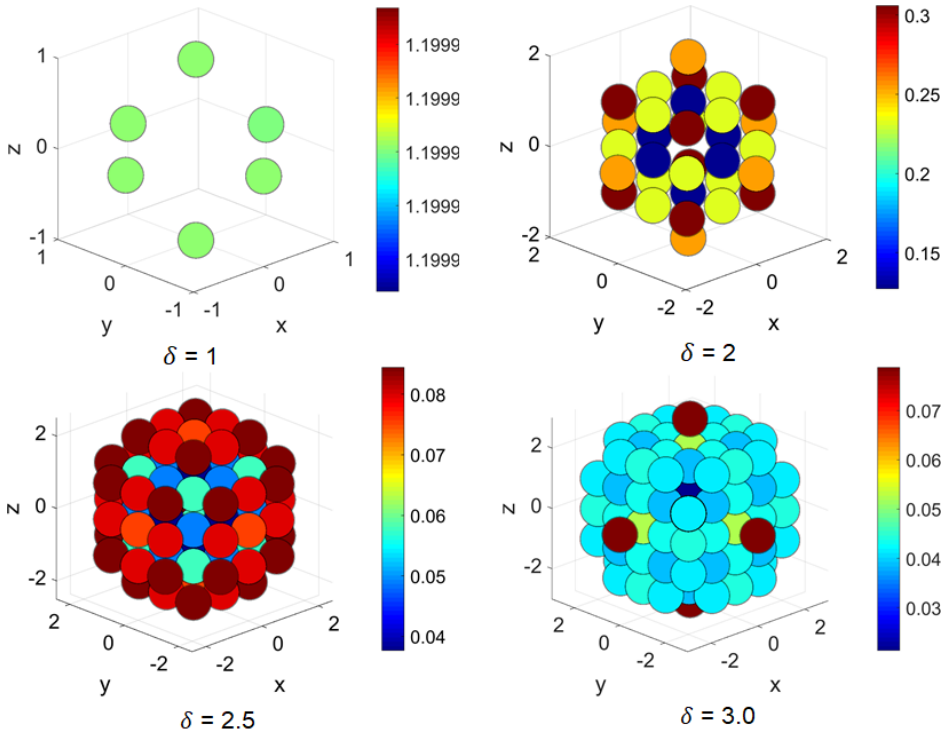

Figure 3: Particle neighborhoods shown for various values of the horizon, $\delta = 1, 2, 2.5$ and 3 considering Young's modulus $E = 1.0$, Poisson's ratio $\nu = 0.25$.

The case with horizon $\delta = 1$ leads to a degenerate solution since the only particles in the neighborhood are the nearest neighbors along the three axes with all bond micromoduli taking the same value of 1.2. Once the bond micromoduli are solved for, the calibrated 'peridynamic stiffness matrix' in Voigt notation can be obtained from the equation

$$\tilde{\mathbf{C}}^{per} = \mathbf{X}\boldsymbol{c}. \tag{49}$$

For $\delta = 1$, the PD stiffness matrix is obtained to be,

$$\mathbf{C}^{per}_{iso} = \begin{bmatrix} 1.2 & 0 & 0 & 0 & 0 & 0 \\ 0 & 1.2 & 0 & 0 & 0 & 0 \\ 0 & 0 & 1.2 & 0 & 0 & 0 \\ 0 & 0 & 0 & 0 & 0 & 0 \\ 0 & 0 & 0 & 0 & 0 & 0 \\ 0 & 0 & 0 & 0 & 0 & 0 \end{bmatrix}. \tag{50}$$

It is observed that in the absence of any bonds apart from the three pairs of bonds along mutually orthogonal axes, the effective PD stiffness matrix only contains axial stiffness terms. This is expected since a pair of bonds along one axis can be deformed without inducing a Poisson's effect or a shear effect. It is also noted that in this simple case, the bond micromodulus is equal to the stiffness terms $c_{11} = c_{22} = c_{33}$ which is fairly straightforward to verify using Eq. (33).

Isotropic, E=1.0, ν=0.25					
Horizon	Min. c	Max. c	c_{an}	Error - LS	Error - An.
1	1.2	1.2	3.8182	0.6325	1.7962
2	0.1271	0.3061	0.2387	2.2981e-15	0.0788
2.5	0.0376	0.0845	0.0978	5.6192e-16	0.3143
3	0.0011	0.0295	0.0052	1.1760e-15	0.1443

Table 1: Minimum and maximum values of the calibrated micromoduli, analytical micromodulus and the errors in the stiffness matrix when using the LS approach and the analytical approach considering Poisson's ratio = 0.25.

In the other cases, PD bonds are able to represent the full stiffness matrix of the reference material. On comparing the two stiffness matrices for the three cases ($\delta = 2, 2.5, 3$), it is seen that an exact solution can be found for all three value of δ, i.e. $\mathbf{C}_{iso}^{per} = \mathbf{C}_{iso}^{ref}$. The relative error in the solution given by $\left\|\tilde{\mathbf{C}}_{iso}^{ref} - \tilde{\mathbf{C}}_{iso}^{per}\right\| / \left\|\tilde{\mathbf{C}}_{iso}^{ref}\right\|$ is given in Table 1 which all appear to be zero to machine precision. The last column in the table also gives the error in the stiffness matrix obtained when the analytical micromodulus is used in Eq. (33). The values of error are stated here to simply illustrate that there can be significant error induced while using the analytical form without any correction, even when the chosen Poisson's ratio is 0.25 (nearly 15%!). This error can be reduced by using volume and surface correction factors which is purposefully not done here [27]. It is to be noted that this error depends on the horizon that is chosen to compute the micromodulus, which here is chosen arbitrarily as the minimum distance required to cover every particle in the lattice. Le and Bobaru [27] have similarly reported the relative difference in the effective peridynamic stiffness and the continuum stiffness for a 2D problem considering $\nu = 1/3$ to be between 0.708% and 0.0146% for different r-ratios, although some volume correction may have been used. While these values are quite low, the LS scheme is able to drive the difference to much lower values, very close to machine precision.

4.2. Poisson's ratio ≠ 0.25

Next, an isotropic material with $E = 1.0$, $\nu = 0.35$ is considered such that the stiffness matrix in Voigt notation is:

$$\mathbf{C}_{iso}^{ref} = \begin{bmatrix} 1.6049 & 0.8642 & 0.8642 & 0 & 0 & 0 \\ 0.8642 & 1.6049 & 0.8642 & 0 & 0 & 0 \\ 0.8642 & 0.8642 & 1.6049 & 0 & 0 & 0 \\ 0 & 0 & 0 & 0.3704 & 0 & 0 \\ 0 & 0 & 0 & 0 & 0.3704 & 0 \\ 0 & 0 & 0 & 0 & 0 & 0.3704 \end{bmatrix}. \tag{51}$$

The LS solution is illustrated in Figure 4 for $\nu = 0.35$ for cases in which a neighborhood is chosen with different values of the horizon, δ.

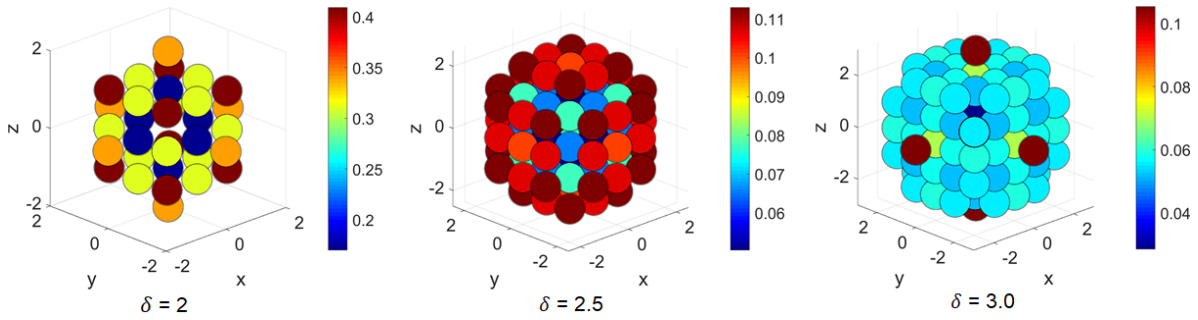

Figure 4: Particle neighborhoods shown for various values of the horizon, $\delta = 2, 2.5$ and 3 considering Young's modulus $E = 1.0$, Poisson's ratio $\nu = 0.35$.

The PD stiffness matrix for all the cases shown in Figure 4 are identical and is given by,

$$\mathbf{C}_{iso}^{per} = \begin{bmatrix} 1.6049 & 0.5350 & 0.5350 & 0 & 0 & 0 \\ 0.5350 & 1.6049 & 0.5350 & 0 & 0 & 0 \\ 0.5350 & 0.5350 & 1.6049 & 0 & 0 & 0 \\ 0 & 0 & 0 & 0.5350 & 0 & 0 \\ 0 & 0 & 0 & 0 & 0.5350 & 0 \\ 0 & 0 & 0 & 0 & 0 & 0.5350 \end{bmatrix}. \tag{52}$$

It is seen that the stiffness terms on the diagonal are obtained exactly equal to the corresponding terms in the reference stiffness matrix. It is also interesting to note that the off diagonal terms c_{12}, c_{23}, c_{13} are equal to the diagonal shear terms c_{44}, c_{55}, c_{66}. It is fairly straightforward to verify by looking at the individual stiffness terms that the effective Poisson's ratio remains 0.25.

Isotropic, E=1.0, ν=0.35					
Horizon	Min. c	Max. c	c_{an}	Error - LS	Error - An.
2	0.1700	0.4094	0.3978	0.2653	0.3455
2.5	0.0503	0.1130	0.1629	0.2653	0.6697
3	0.0284	0.1054	0.0786	0.2653	0.4751

Table 2: Minimum and maximum values of the calibrated micromoduli, analytical micromodulus and the errors in the stiffness matrix when using the LS approach and the analytical approach considering Poisson's ratio = 0.35.

Table 2 presents the minimum and maximum values of bond micromoduli, the analytical micromodulus, and the errors in the solution obtained from using the LS approach and the analytical micromodulus, for three values of horizon. It is seen that the error obtained from the LS approach, while significant, remains constant for different values of the horizon. However, the error varies from ~0.35 to ~0.67 while using the constant analytical micromodulus. This can again be attributed to volume effects due to the discrepancy in the spherical volume considered while calculating the analytical micromodulus and the actual volume occupied by all particles.

The LS approach is also used for cases in which Poisson's ratio $0.05 \leq \nu \leq 0.45$, considering $\delta = 3$, results of which are given in Table 3.

Isotropic, δ = 3 for varying Poisson's ratio					
Poisson's Ratio	Min. c	Max. c	c_{an}	Error - LS	Error - An.
0.05	0.0178	0.0660	0.0262	0.3524	0.4293
0.15	0.0187	0.0693	0.0337	0.2059	0.2326
0.25	0.0011	0.0295	0.0052	4.4774e-16	0.1443
0.35	0.0284	0.1054	0.0786	0.2653	0.4751
0.45	0.0672	0.2491	0.2358	0.5453	0.8533

Table 3: Minimum and maximum values of the calibrated micromoduli, analytical micromodulus and the errors in the stiffness matrix when using the LS approach and the analytical approach considering Poisson's ratio = 0.05 - 0.45.

For $\nu = 0.25$, the solution is exact, and the error in the LS solution is zero, where as the error is significant for other values, ranging from 0.3524 for $\nu = 0.05$ to 0.5453 for $\nu = 0.45$. The error in the PD stifness matrix when using an analytical value for the micromodulus is also given, and is quite significant in all cases, being larger than the error obtained when using the LS approach. It is to be noted that this error is both due to volume effects and due to the shortcomings of the bond-based PD model when choosing a Poisson's ratio other than 0.25. Therefore by eliminating the error due to volume effects by using the LS approach, the residual error is purely due to the limitation of the bond-based model.

4.3. Surface corrections

The same calibration scheme used in the bulk can be applied to neighborhoods at the surface as well. Figure 5 shows a typical neighborhood at a face, edge and a corner of a uniformly discretized 3D domain. For all cases, the Young's modulus is set to 1.0 and Poisson's ratio is set to 0.25 and the horizon is chosen to be 3.

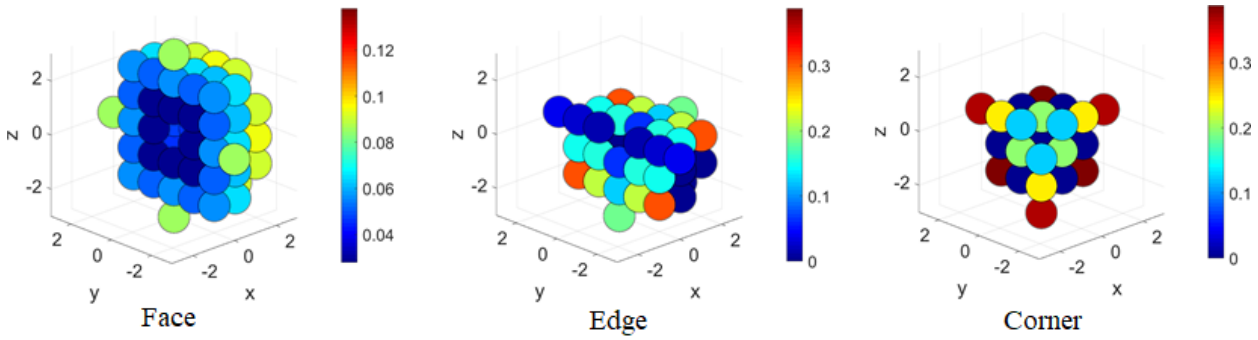

Figure 5: Particle neighborhoods shown for surfaces - at a face, edge and a corner considering Young's modulus $E = 1.0$, Poisson's ratio $\nu = 0.25$ and horizon $\delta = 3$

As seen from Figure 5 and Table 4, a solution can be obtained using the same scheme, however with mixed success. For instance, the error in the solution when calibrating for a face is zero meaning that the peridynamic stiffness can be matched exactly to the material stiffness. The error using the anaytical micromodulus without any correction is ~0.34, therefore a big improvement can be achieved with the LS scheme. However the error is quite large, 0.2760 and 0.4781 for the edge and corner cases respectively albeit still lesser than the error obtained using simply the analytical micromodulus. As seen in Le et al. [27], some other surface correction schemes produce far lesser errors at corners in terms of the displacement. It is also notable that for the edge and corner cases, the minimum micromodulus obtained is zero although it is unclear why this occurs. For practical purposes, it may be possible to set a lower bound on the micromodulus during step 2 of the calibration (when solving the quadratic program) although it is not attempted here.

Isotropic, E=1.0, ν=0.25, δ=3					
Type	Min. c	Max. c	c_{an}	Error - LS	Error - An.
Face	0.0278	0.1380	0.0472	2.0536e-16	0.3395
Edge	0.0	0.3879	0.0472	0.2760	0.6205
Corner	0.0	0.3879	0.0472	0.4781	0.7781

Table 4: Minimum and maximum values of the calibrated micromoduli, analytical micromodulus and the errors in the stiffness matrix when using the LS approach and the analytical approach for face, edge and corner cases, E=1.0, ν=0.35, δ=3.

We also present some details on different values of Poisson's ratio when calibrating for a face case. The distribution of micromoduli values appear quite similar to Figure 5. The error obtained from the LS scheme remains the same as the error obtained in the bulk, i.e. the errors provided in Table 3. Again, there errors are significant, up to 0.5453 when ν is equal to 0.45, however they still remain smaller than the errors obtained when using the analytical micromodulus. Interestingly, the error when using the conventional approach has more than doubled from that obtained in the bulk. e.g. the error in the bulk for $\nu = 0.25$ is $\sim 15\%$ where as that for a face is $\sim 34\%$.

Face, Isotropic, $\delta = 3$ for varying Poisson's ratio					
Poisson's Ratio	Min. c	Max. c	c_{an}	Error - LS	Error - An.
0.05	0.0233	0.1156	0.0262	0.3524	0.6283
0.15	0.0245	0.1215	0.0337	0.2059	0.4938
0.25	0.0011	0.0295	0.0052	2.0536e-16	0.3395
0.35	0.0372	0.1846	0.0786	0.2653	0.3292
0.45	0.0880	0.4364	0.2358	0.5453	0.5647

Table 5: Minimum and maximum values of the calibrated micromoduli, analytical micromodulus and the errors in the stiffness matrix when using the LS approach and the analytical approach for the face case, considering Poisson's ratio = 0.05 - 0.45, E=1.0, δ=3.

The edge and corner cases have not been delved into further because of the impractically high errors even for the case where $\nu = 0.25$. It is expected that the calibration scheme will be further refined in the future to improve these errors.

5. Summary and Conclusions

A novel least squares approach to calibrating micromoduli in a discrete setting is proposed. Unlike using an analytical equation to find the micromodulus using strain energy equivalence, the micromoduli are calibrated such that the effective peridynamic stiffness matrix is closest to the reference stiffness matrix in a least squares sense. To account for the fact that the micromoduli have to be non-negative, a correction scheme is proposed which is cast as a quadratic program. Results for a local neighborhood, both in the bulk and at a surface for an isotropic material are shown. Comparison of the error in the stiffness matrix when using the conventional approach and the least squares approach shows a significant reduction in error. For example, even in the case where $\nu = 0.25$, the error in calibration can be reduced from $\sim 15\%$ to effectively 0. As part of ongoing work, more investigation into anisotropy, irregular discretization and surface effects will be considered in future work.

References

[1] Stewart A Silling. Reformulation of elasticity theory for discontinuities and long-range forces. *Journal of the Mechanics and Physics of Solids*, 48(1):175–209, 2000.

[2] Florin Bobaru and Monchai Duangpanya. The peridynamic formulation for transient heat conduction. *International Journal of Heat and Mass Transfer*, 53(19):4047–4059, 2010.

[3] Bahattin Kilic and Erdogan Madenci. Peridynamic theory for thermomechanical analysis. *Advanced Packaging, IEEE Transactions on*, 33(1):97–105, 2010.

[4] Naveen Prakash and Gary D Seidel. Electromechanical peridynamics modeling of piezoresistive response of carbon nanotube nanocomposites. *Computational Materials Science*, 113:154–170, 2016.

[5] Walter Gerstle, Stewart Silling, David Read, Vinod Tewary, and Richard Lehoucq. Peridynamic simulation of electromigration. *Comput Mater Continua*, 8(2):75–92, 2008.

[6] Amit Katiyar, John T Foster, Hisanao Ouchi, and Mukul M Sharma. A peridynamic formulation of pressure driven convective fluid transport in porous media. *Journal of Computational Physics*, 261:209–229, 2014.

[7] Ziguang Chen and Florin Bobaru. Peridynamic modeling of pitting corrosion damage. *Journal of the Mechanics and Physics of Solids*, 78:352–381, 2015.

[8] Youn Doh Ha and Florin Bobaru. Studies of dynamic crack propagation and crack branching with peridynamics. *International Journal of Fracture*, 162(1-2):229–244, 2010.

[9] Bahattin Kilic and Erdogan Madenci. Prediction of crack paths in a quenched glass plate by using peridynamic theory. *International journal of fracture*, 156(2):165–177, 2009.

[10] Ebrahim Askari, Jifeng Xu, and Stewart Silling. Peridynamic analysis of damage and failure in composites. In *44th AIAA Aerospace Sciences Meeting and Exhibit, Reno, Nevada. Reston, VA: AIAA*, 2006.

[11] Walter Gerstle, Nicolas Sau, and SA Silling. Peridynamic modeling of plain and reinforced concrete structures. In *SMiRT18: 18th lnt. Conf. Struct. Mech. React. Technol., Beijing*, 2005.

[12] Naveen Prakash and Gary D Seidel. Computational electromechanical peridynamics modeling of strain and damage sensing in nanocomposite bonded explosive materials (ncbx). *Engineering Fracture Mechanics*, 2017.

[13] Hisanao Ouchi, Amit Katiyar, John Foster, Mukul Mani Sharma, et al. A peridynamics model for the propagation of hydraulic fractures in heterogeneous, naturally fractured reservoirs. In *SPE Hydraulic Fracturing Technology Conference*. Society of Petroleum Engineers, 2015.

[14] Naveen Prakash. *Coupled Electromechanical Peridynamics Modeling of Strain and Damage Sensing in Carbon Nanotube Reinforced Polymer Nanocomposites*. PhD thesis, Virginia Tech, 2017.

[15] SA Silling and RB Lehoucq. Peridynamic theory of solid mechanics. *Advances in Applied mechanics*, 44:73–168, 2010.

[16] Stewart A Silling and Ebrahim Askari. A meshfree method based on the peridynamic model of solid mechanics. *Computers & Structures*, 83(17):1526–1535, 2005.

[17] Gao-Feng Zhao, Jiannong Fang, and Jian Zhao. A 3d distinct lattice spring model for elasticity and dynamic failure. *International Journal for Numerical and Analytical Methods in Geomechanics*, 35(8):859–885, 2011.

[18] Gavin A Buxton, Christopher M Care, and Douglas J Cleaver. A lattice spring model of heterogeneous materials with plasticity. *Modelling and simulation in materials science and engineering*, 9(6):485, 2001.

[19] A Jagota and SJ Bennison. Spring-network and finite-element models for elasticity and fracture. In *Non-linearity and Breakdown in Soft Condensed Matter*, pages 186–201. Springer, 1994.

[20] Anand Jagota and George W Scherer. Viscosities and sintering rates of a two-dimensional granular composite. *Journal of the American Ceramic Society*, 76(12):3123–3135, 1993.

[21] Youn Doh Ha and Florin Bobaru. Characteristics of dynamic brittle fracture captured with peridynamics. *Engineering Fracture Mechanics*, 78(6):1156–1168, 2011.

[22] Richard W Macek and Stewart A Silling. Peridynamics via finite element analysis. *Finite Elements in Analysis and Design*, 43(15):1169–1178, 2007.

[23] Erkan Oterkus. Peridynamic theory for modeling three-dimensional damage growth in metallic and composite structures. 2010.

[24] Erdogan Madenci and Erkan Oterkus. *Peridynamic theory and its applications*, volume 17. Springer, 2014.

[25] Florin Bobaru, John T Foster, Philippe H Geubelle, and Stewart A Silling. *Handbook of Peridynamic Modeling*. CRC Press, 2016.

[26] John Mitchell, Stewart Silling, and David Littlewood. A position-aware linear solid constitutive model for peridynamics. *Journal of Mechanics of Materials and Structures*, 10(5):539–557, 2015.

[27] QV Le and F Bobaru. Surface corrections for peridynamic models in elasticity and fracture. *Computational Mechanics*, pages 1–20, 2017.
[28] Florin Bobaru and Youn Doh Ha. Adaptive refinement and multiscale modeling in 2d peridynamics. *International Journal for Multiscale Computational Engineering*, 9(6), 2011.
[29] Michael L Parks, Pablo Seleson, Steven J Plimpton, Richard B Lehoucq, and Stewart A Silling. Peridynamics with lammps: A user guide v0. 2 beta. *Sandia Report*, pages 1–20, 2008.
[30] Pablo Seleson. Improved one-point quadrature algorithms for two-dimensional peridynamic models based on analytical calculations. *Computer Methods in Applied Mechanics and Engineering*, 282:184–217, 2014.
[31] Pablo Seleson and David J Littlewood. Convergence studies in meshfree peridynamic simulations. *Computers & Mathematics with Applications*, 71(11):2432–2448, 2016.
[32] Wenyang Liu and Jung-Wuk Hong. Discretized peridynamics for brittle and ductile solids. *International Journal for Numerical Methods in Engineering*, 89(8):1028–1046, 2012.
[33] Wenyang Liu and Jung-Wuk Hong. Discretized peridynamics for brittle and ductile solids. *International Journal for Numerical Methods in Engineering*, 89(8):1028–1046, 2012.
[34] Georg C Ganzenmüller, Stefan Hiermaier, and Michael May. Improvements to the prototype micro-brittle model of peridynamics. In *Meshfree methods for partial differential equations VII*, pages 163–183. Springer, 2015.

Appendix A. Rotational symmetry

It is also noted that the neighborhoods formed have some discrete rotational symmetries, e.g. rotations of $\pi/2$ about any of the axes will result in no difference with respect to bond micromoduli. Therefore this satisfies the requirement on individual bonds for isotropic symmetry, at least in a discrete sense just by visual inspection, as given in [1].

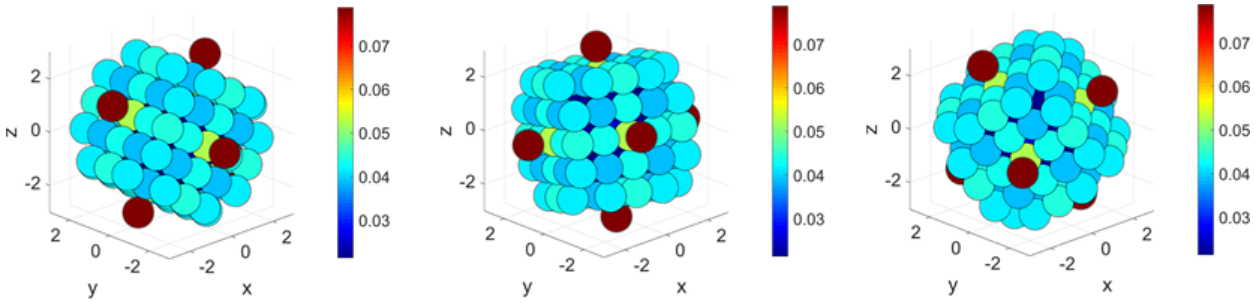

Figure A.6: Particle neighborhoods after arbitrary rotations considering Young's modulus $E = 1.0$, $E = 1.0$, Poisson's ratio $\nu = 0.25$ and horizon $\delta = 3$

Arbitrary rotations of the neighborhood of particles about all three axes also result in the same stiffness matrix with respect to the reference coordinate system with the difference being on the order of machine precision. Figure A.6 shows some of the configurations tested. Similar results were obtained for neighborhoods of different horizon values, Poisson's ratio and even surface neighborhoods.